Journal of Magnetism and Magnetic Materials 648 (2026) 174091

Contents lists available at ScienceDirect

Journal of Magnetism and Magnetic Materials

journal homepage: www.elsevier.com/locate/jmmm

Research article

Angular dependence of stress-induced spin-wave dynamics in antivortices stabilized in square FeGa nanodots

Eduardo Saavedra [a], Helmunt Vigo-Cotrina [b], Mohammed Al Bahri [e], Laura M. Pérez [c], Felipe Tejo [d],*

[a] *Departamento de Física, Universidad de Santiago de Chile, Avda. Víctor Jara 3493, 9170124 Santiago, Chile*
[b] *Centro de Investigación en Nanotecnología y Materiales Avanzados (CINMA), Universidad Privada del Norte (UPN), Peru*
[c] *Department of Basic and Applied Sciences, A'Sharqiyah University, Post Box 42, PC 400, Ibra, Oman*
[d] *Departamento de Ingeniería Industrial y de Sistemas, Universidad de Tarapacá, Casilla 7D, 1000000 Arica, Chile*
[e] *Vicerrectoría de Investigación, Innovación y Postgrado, Universidad Central de Chile, Santiago, Chile*

ARTICLE INFO

Keywords:
Magnetic antivortices
Spin-wave dynamics
Strain-controlled magnetism
FeGa nanodots

ABSTRACT

We investigate the angular dependence of stress-induced spin-wave dynamics in magnetic antivortices stabilized in square FeGa nanodots by means of micromagnetic simulations. The application of in-plane uniaxial stress generates an effective magnetoelastic anisotropy whose magnitude and orientation are systematically varied to analyze their impact on the stability, core position, and dynamic response of the antivortex state. A magnetic state diagram reveals well-defined regions where the antivortex remains stable, as well as angular and stress thresholds beyond which the configuration becomes unstable and relaxes into a different magnetic state. Within the stable regime, the antivortex core undergoes pronounced angular-dependent displacements, reflecting the strong sensitivity of the antivortex topology to the orientation of the applied stress. Ferromagnetic resonance analysis shows that the spin-wave spectrum exhibits a multibranch structure composed of discrete modes whose frequencies, intensities, and angular dispersion are strongly modulated by the stress orientation. At higher stress amplitudes, the spectra display enhanced angular modulation, mode hybridization, and the emergence of instability-induced spectral fragmentation. Spatial mode analysis reveals a rich variety of excitations ranging from core-localized modes to extended standing-wave patterns governed by the combined effects of square confinement and angular magnetoelastic anisotropy. These results demonstrate that angular stress tuning provides an efficient and energy-efficient route to control antivortex stability and spin-wave dynamics, opening new perspectives for reconfigurable magnonic devices based on topological magnetic textures.

1. Introduction

The control of spin-wave dynamics in confined magnetic nanostructures is a central topic in modern magnonics, motivated by the growing demand for low-power, compact, and reconfigurable platforms operating in the gigahertz frequency range [1,2]. Spin waves provide an attractive route for information transport and processing without charge motion, enabling reduced energy dissipation compared to conventional electronic approaches. Consequently, considerable effort has been devoted to identifying efficient mechanisms capable of tailoring magnetic excitations in nanoscale systems while preserving scalability and energy efficiency.

Among the different strategies explored to manipulate magnetization dynamics, mechanical stress has emerged as a particularly powerful and versatile control parameter. Through magnetoelastic coupling, applied strain induces an effective magnetic anisotropy that modifies both the static magnetic configuration and the dynamic response of magnetostrictive materials. In contrast to magnetic-field [3,4]- or current-driven approaches [5], stress-induced control is inherently energy efficient and nonvolatile, while also avoiding Joule heating [6,7]. These advantages have positioned strain-mediated magnetism at the core of magnetic straintronics [8,9] and flexible magnonic systems [1,10].

In addition to conventional magnetoelastic anisotropy, strain may also modify other magnetic interaction terms. In particular, recent

* Corresponding author.
E-mail address: felipe.tejo@ucentral.cl (F. Tejo).

https://doi.org/10.1016/j.jmmm.2026.174091
Received 7 February 2026; Received in revised form 31 March 2026; Accepted 2 April 2026
Available online 3 April 2026

studies have shown that lattice distortions can induce anisotropic contributions to the Dzyaloshinskii–Moriya interaction (DMI), leading to complex domain structures in systems where strong spin–orbit coupling is present. For instance, Sapozhnikov et al. demonstrated that strain-induced anisotropy of DMI can produce zigzag magnetic domains in chiral systems [11]. However, in magnetostrictive materials such as FeGa without heavy-metal interfaces, strain effects are typically dominated by magnetoelastic energy contributions. Recent theoretical studies have further shown that electric-field-induced strain in hybrid multiferroic heterostructures can also modulate the interfacial Dzyaloshinskii–Moriya interaction (DMI), providing an additional route for controlling chiral magnetic textures through voltage-driven strain [12]. Experimental evidence of this mechanism has also been reported in heavy-metal/ferromagnet multilayers, where uniaxial strain was shown to reversibly modify the interfacial DMI constant in Co/Pt systems, demonstrating the feasibility of strain-driven control of chiral interactions in thin films [13].

FeGa alloys are especially attractive for strain-controlled magnonic applications [14–18], due to their large magnetostriction coefficient, low magnetic damping, and favorable mechanical properties. These characteristics have enabled extensive investigations of stress-tunable magnetization dynamics in a wide range of systems, including continuous films [15], stripes [17], nanodots [16,19], nanorings [14], and geometrically engineered two-dimensional nanostructures [18]. Previous studies have demonstrated that stress-induced anisotropy can strongly modify ferromagnetic resonance frequencies, dynamic susceptibility, and spin-wave mode profiles, providing efficient spectral reconfiguration across the gigahertz range. In confined nanostructures, the interplay between geometry, dipolar interactions, and magnetoelastic effects gives rise to rich and highly tunable spin-wave spectra.

Within this context, magnetic vortices have been extensively studied as prototypical topological textures stabilized by geometric confinement. Their dynamic excitations, including gyrotropic, azimuthal, and breathing modes, are now well understood [20] and can be efficiently tailored through geometry, material parameters, external magnetic fields, and mechanical stress. In particular, recent works [16,19] on FeGa-based nanostructures have demonstrated that strain-induced anisotropy strongly modifies both the resonance frequencies and spatial profiles of vortex spin-wave modes, enabling dynamic reconfiguration of their microwave response.

Topological magnetic textures, including vortices, skyrmions, and antivortices have attracted considerable attention due to their stability and unique dynamical properties. In particular, the stabilization and nucleation of skyrmions in confined nanostructures have been widely investigated, where geometrical confinement and the interplay between exchange, dipolar interactions, and anisotropy play a crucial role [21,22].

In contrast, magnetic antivortices, which are the topological counterparts of vortices, have received considerably less attention, especially regarding their dynamic properties. Antivortices are characterized by an opposite winding number and an in-plane magnetization pattern with converging and diverging components, leading to enhanced magnetostatic charges and reduced intrinsic stability. These features make their stabilization challenging and highly sensitive to geometry and symmetry. Only recently have micromagnetic studies [23–25] demonstrated that antivortices can be stabilized in carefully designed nanostructures and can support distinct spin-wave excitations that do not have a direct analogue in vortex systems.

Despite these advances, the influence of mechanical stress on antivortex spin-wave dynamics remains largely unexplored. Existing studies have primarily focused on field-driven excitations or geometrical stabilization mechanisms, leaving open fundamental questions regarding how stress-induced anisotropy affects antivortex stability and dynamics. This issue is particularly relevant given the reduced symmetry and anisotropic magnetization distribution of antivortices, which suggest an enhanced sensitivity not only to the magnitude but also to the in-plane orientation of externally applied stress.

In this work, we investigate the angular dependence of stress-induced spin-wave dynamics in antivortices stabilized in square FeGa nanodots using micromagnetic simulations. By systematically varying both the magnitude and the orientation of the applied uniaxial stress, we demonstrate that angular stress tuning provides an efficient control mechanism to reshape the spin-wave spectra, spatial mode profiles, and stability of antivortex configurations. Our results reveal a strong interplay between antivortex topology, geometric confinement, and angular magnetoelastic anisotropy. These findings establish angular stress as a versatile and energy-efficient parameter for controlling antivortex dynamics and open new perspectives for reconfigurable magnonic devices and spin-wave-based information processing architectures [26].

2. Micromagnetic simulations

We performed micromagnetic simulations using the MuMax3 software package [27], which numerically solves the Landau–Lifshitz–Gilbert (LLG) equation [28],

$$\frac{d\mathbf{M}}{dt} = -\gamma\left(\mathbf{M}\times\mathbf{H}_{\mathrm{eff}}\right) + \frac{\alpha}{M_s}\left(\mathbf{M}\times\frac{d\mathbf{M}}{dt}\right), \tag{1}$$

where γ and α denote the gyromagnetic ratio and the Gilbert damping constant, respectively. The vector $\mathbf{M}$ represents the magnetization, and $\mathbf{H}_{\mathrm{eff}}$ is the effective magnetic field, including exchange, dipolar, Zeeman, and stress-induced uniaxial anisotropy contributions. Surface anisotropy was not explicitly included in the simulations, as the magnetic configuration of the nanodot is primarily governed by exchange and magnetostatic interactions associated with the lateral confinement of the structure.

The simulations were performed using an exchange stiffness $A = 14\times10^{-12}$ J,m^{-1} and a saturation magnetization $M_s = 1350\times10^3$ A,m^{-1}, corresponding to typical magnetic parameters of FeGa. Angular stress tuning was implemented by applying an in-plane uniaxial stress to the square FeGa nanodots. The stress orientation, defined by the angle θ, was swept from 0° to 90° in steps of 5°, while the stress magnitude σ was varied from 0 to 150 MPa in increments of 5 MPa.

The resulting stress-induced anisotropy (K_σ) was modeled through an effective uniaxial anisotropy constant by the expression [16,17,29,30]

$$K_\sigma = \frac{3}{2}\lambda_s\sigma, \tag{2}$$

where the magnetostriction coefficient was taken as $\lambda_s = 260$ ppm.

In the simulations, the effect of the applied stress is incorporated as an additional uniaxial magnetoelastic anisotropy. Although small strain relaxation may occur near the edges of patterned structures due to substrate clamping or boundary effects, elastic simulations indicate that the strain distribution remains nearly uniform over most of the interior region of the magnetic element [31]. Given that the antivortex core dynamics and the spin-wave modes analyzed in this work are mainly governed by the magnetization distribution in the interior of the nanodot, these edge-related variations are expected to have only a minor influence on the results. Therefore, the strain-induced contribution is modeled here as a spatially uniform anisotropy term, a commonly adopted approximation in micromagnetic studies of strain-mediated magnetization dynamics [32,33]. No additional intrinsic magnetocrystalline anisotropy was included, in order to isolate the role of the stress-induced magnetoelastic anisotropy. This assumption is justified by the polycrystalline nature of the FeGa nanostructures, where magnetocrystalline contributions are typically averaged out and remain smaller than the stress-induced anisotropy within the range of parameters considered [17,18].

The system under investigation consists of a square FeGa nanodot with lateral size $L = 200$ nm and thickness $h = 5$ nm, discretized into cubic cells of $1\times1\times1$ nm^3 in order to accurately resolve the relevant micromagnetic features. The mesh size used in the simulations was chosen to be smaller than the characteristic magnetic length scales of FeGa.

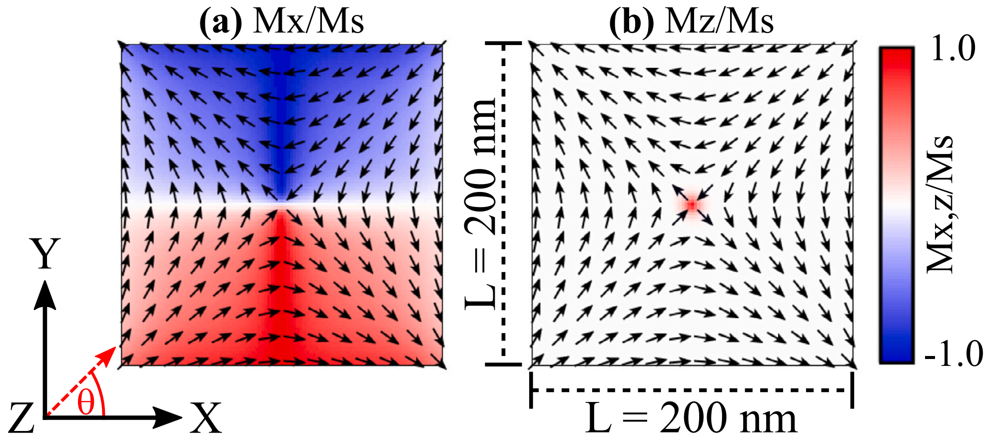

Fig. 1. Equilibrium magnetization configuration of an antivortex stabilized in a square FeGa nanodot obtained from micromagnetic simulations. The nanodot has lateral size $L = 200$ nm and thickness $h = 5$ nm. The arrows represent the in-plane magnetization components, while the color map shows the normalized magnetization components M_x/M_s (left panel) and M_z/M_s (right panel), as indicated by the color scale. The antivortex core is visible as a localized red region at the center of the nanodot. The angle θ defines the in-plane orientation of the applied uniaxial stress with respect to the x axis. The configuration corresponds to the stress-free case ($\sigma = 0$ MPa).

In particular, the exchange length $l_{ex} = \sqrt{2A/(\mu_0 M_s^2)}$ is approximately 3–4 nm. Additionally, the anisotropy exchange length $l_K = \sqrt{A/K}$ was evaluated using the maximum stress-induced anisotropy considered in this study ($K \approx 5.85 \times 10^4$ J/m^3 for $\sigma = 150$ MPa), yielding $l_K \approx 49$ nm. These values confirm that the chosen discretization is sufficiently fine to accurately resolve the domain-wall structure and the antivortex core.

The antivortex configurations were stabilized through a two-step relaxation procedure. Initial magnetization state were generated using the built-in MuMax3 function m = antivortex(1,1), which produces a well-defined antivortex configuration with prescribed circulation and core polarization. This state were subsequently relaxed under zero external magnetic field using an enhanced damping constant $\alpha = 0.5$, and the relaxation process was terminated when the maximum torque acting on the magnetic moments dropped below 10^{-4}T [34,35].

After static relaxation, the resulting configurations were further evolved dynamically by solving the Landau–Lifshitz–Gilbert (LLG) equation in the absence of external fields for 100 ns. This time interval is sufficient to ensure the decay of residual spin-wave excitations [36] and to confirm the temporal stability of the antivortex state. Fig. 1 shows the relaxed magnetic configuration of the antivortex state for the stress-free case ($\sigma = 0$ MPa). The color scale represents the normalized x- and z-components of the magnetization, while the arrows indicate the in-plane magnetization direction. The antivortex core is visible as a localized red region at the center of the nanodot, as highlighted in Fig. 1(b). The angle θ defines the in-plane orientation of the applied uniaxial stress with respect to the x axis.

The final magnetic configuration obtained after the dynamic relaxation stage was subsequently used as the equilibrium state for the ferromagnetic resonance (FMR) analysis. Ferromagnetic resonance techniques are widely used to characterize spin-wave excitations and standing spin-wave modes in nanostructured magnetic systems [37]. To excite the system and probe its dynamic response, a time-dependent magnetic field pulse $\mathbf{h}(t)$ was applied along the out-of-plane direction, defined as $\mathbf{h}(t) = h_0 \,\mathrm{sinc}\left[2\pi f_c(t - t_0)\right] \hat{\mathbf{z}}$, where $h_0 = 1$ mT is the field amplitude, $f_c = 40$ GHz is the cutoff frequency, and $t_0 = 1$ ns is the pulse delay. For the dynamic simulations and the FMR spectral analysis, a Gilbert damping constant of $\alpha = 0.01$ was used. The spatial distribution of the magnetization was recorded every 10 ps over a total simulation time of 100 ns, resulting in a frequency resolution of 0.01 GHz.

After this process, the time-dependent magnetic field $h(t)$ and the magnetization distribution $M(t)$ were transformed into the frequency domain, $h(\omega)$ and $M(\omega)$, using the Fast Fourier Transform (FFT). The dynamic susceptibility was then obtained as the ratio between the Fourier components of the magnetization response and the excitation field, $\chi(\omega) = M(\omega)/h(\omega)$, and its imaginary part was used to characterize the ferromagnetic resonance spectrum.

To gain further insight into the origin of the resonance peaks, the spatial profiles of the spin-wave modes were extracted by performing a temporal Fourier transform of the magnetization dynamics at each simulation cell, $m(\mathbf{r}_{ijk})$, according to $\omega_n = \mathrm{DFTt}(m(r_i jk, t_n))$. Here, DFT$_t$ denotes the discrete-time Fourier transform, the subscript ijk labels the spatial coordinates (x, y, z) of each discretization cell, and n indexes the frequency components of the power spectrum. This spatially resolved spectral analysis allows the construction of mode maps, providing direct insight into the spatial distribution, localization, and propagation characteristics of the excited spin-wave modes.

3. Results and discussion

First, a magnetic state diagram was obtained by systematically varying the stress orientation θ and magnitude σ, starting from an initial antivortex (AV) configuration, as shown in Fig. 1. This analysis focuses exclusively on the stability of the antivortex state. The resulting phase diagram, presented in Fig. 2(a), summarizes the final magnetic configurations as a function of θ and σ. The red region identifies parameter combinations for which the antivortex remains stable after relaxation, whereas the blue region denotes cases in which the initial AV configuration becomes unstable and relaxes into a different equilibrium magnetic state. The critical angle θ separating these regimes is strongly dependent on the applied stress magnitude σ.

Representative equilibrium magnetization configurations for selected stress values $\sigma = 25$, 50, 100, and 125 MPa and different stress orientations θ are presented in Fig. S1 of the Supplemental Material. In these maps, the color scale represents the normalized out-of-plane magnetization component M_z/M_s, while the arrows indicate the in-plane magnetization direction. These configurations reveal that the antivortex core progressively shifts away from the center of the nanodot as θ and σ are varied. For stress values approaching the instability boundary identified in the phase diagram, the antivortex core is displaced toward the edges of the nanodot and the magnetization distribution becomes increasingly distorted. Beyond the stability threshold, the system relaxes into non-antivortex configurations characterized by strongly nonuniform in-plane magnetization patterns without a well-defined topological core.

To quantify this behavior, the trajectory of the antivortex core position was extracted and is shown in Fig. 2(b). The core position

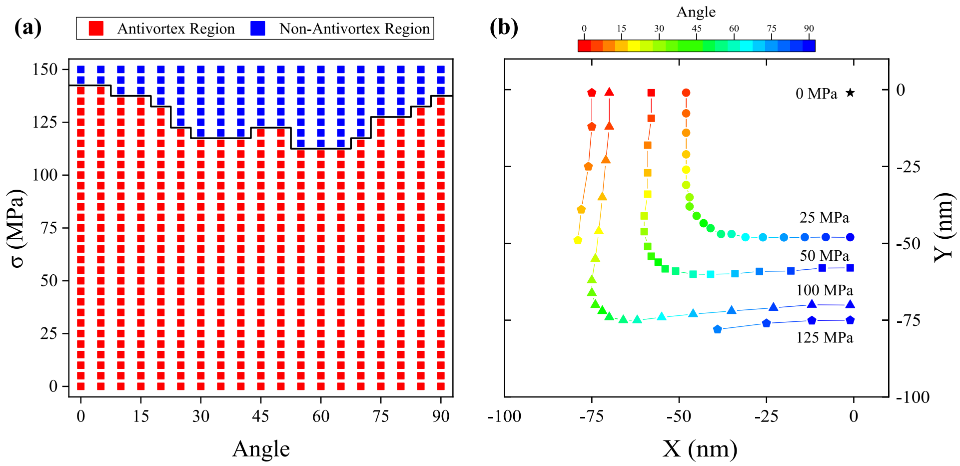

Fig. 2. (a) Magnetic state diagram as a function of the stress orientation angle θ and stress magnitude σ, obtained by relaxing an initial antivortex configuration. The red region indicates parameter combinations for which the antivortex state remains stable, while the blue region ("non-antivortex region") corresponds to cases where the initial antivortex configuration becomes unstable and relaxes into a different equilibrium magnetic state. (b) Trajectories of the antivortex core position in the xy plane for selected stress magnitudes σ = 25, 50, 100, and 125 MPa as a function of the stress orientation θ. The color scale encodes the value of θ, highlighting the angular dependence of the core displacement.

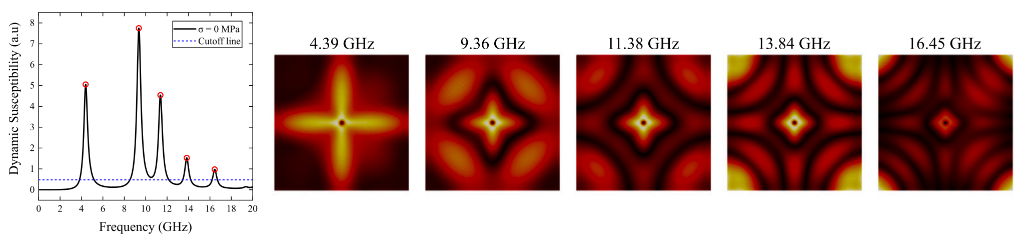

Fig. 3. Spin-wave spectra and mode profiles of the antivortex configuration in a square FeGa nanodot for the stress-free case (σ = 0 MPa). Left panel: imaginary part of the dynamic susceptibility as a function of frequency, showing discrete resonance peaks. The horizontal dashed blue line indicates the cutoff threshold set to 4% of the maximum peak intensity, used to identify the dominant modes. Right panels: spatial distributions of the normalized FFT amplitude extracted from the magnetization dynamics at the selected resonance frequencies (4.39, 9.36, 11.38, 13.84, and 16.45 GHz). The mode profiles correspond to radial (breathing-type) excitations of the antivortex core with increasing spatial complexity and a growing number of diagonal nodal lines.

was determined from the spatial distribution of the out-of-plane magnetization component M_z, identifying the location where $|M_z|$ reaches its maximum value, which corresponds to the center of the antivortex core, as illustrated in Fig. S1 of the Supplementary Material. Although the antivortex core may exhibit a diffuse profile, the maximum of $|M_z|$ remains well localized within a small region, allowing for a robust determination of the core position. The results demonstrate that the core displacement follows distinct angular-dependent paths for different stress magnitudes, indicating that the combined action of stress amplitude and orientation provides an efficient mechanism to control both the stability and spatial position of the antivortex core within the nanodot.

To further understand the stability thresholds observed in the magnetic state diagram, we analyzed the individual energy contributions associated with the equilibrium configurations. The exchange, dipolar, and anisotropy energies as a function of the stress orientation angle θ for representative stress values are presented in Fig. S2 of the Supplementary Material.

The results show that, for low and intermediate stress amplitudes (σ = 25–100 MPa), the different energy contributions remain relatively stable as a function of θ, which is consistent with the robustness of the antivortex state in this regime. In contrast, for higher stress values (σ = 125 MPa), pronounced variations in the dipolar and anisotropy energies are observed, particularly around intermediate angles. This behavior reflects an increased competition between these energy terms, which destabilizes the antivortex configuration and is consistent with the instability region identified in the phase diagram (Fig. 2(a)).

Fig. 3 shows the spin-wave spectra of the antivortex configuration in a square FeGa nanodot for the stress-free case (σ = 0 MPa), excited by an out-of-plane magnetic field pulse. Before analyzing the spectral features in detail, we verified that the obtained resonances are robust with respect to the value of the damping parameter used in the dynamic simulations. Additional calculations were performed using different damping constants (α = 0.01–0.025). The results, presented in Fig. S4 of the Supplementary Material, show that increasing the damping reduces the peak amplitude and broadens the spectral linewidth, while the resonance frequencies remain essentially unchanged. The frequency spectrum, obtained from the imaginary part of the dynamic susceptibility, exhibits a discrete set of well-defined resonance peaks. To ensure a consistent identification of the dominant modes, a cutoff threshold corresponding to 4% of the amplitude of the highest-intensity resonance was applied and is indicated by the horizontal dashed blue line (See Fig. S3 of the Supplementary Material).

Five resonant modes are clearly observed at frequencies of 4.39, 9.36, 11.38, 13.84, and 16.45 GHz. These modes are associated with radial (breathing-type) excitations of the antivortex core, characterized by increasing frequency and spatial complexity. To elucidate the origin of these resonances, the right panels of Fig. 3 display the spatial distributions of the normalized FFT amplitude extracted from the magnetization dynamics at the corresponding frequencies. The mode profiles reveal a progressive increase in the number of nodal lines along the diagonals of the nanodot, allowing the modes to be classified by an integer index n = 1, 2,3, 4 and 5, corresponding to diagonal standing-wave patterns with increasing order [23,38,39]. These nodal patterns reflect the underlying symmetry of the system. In the absence

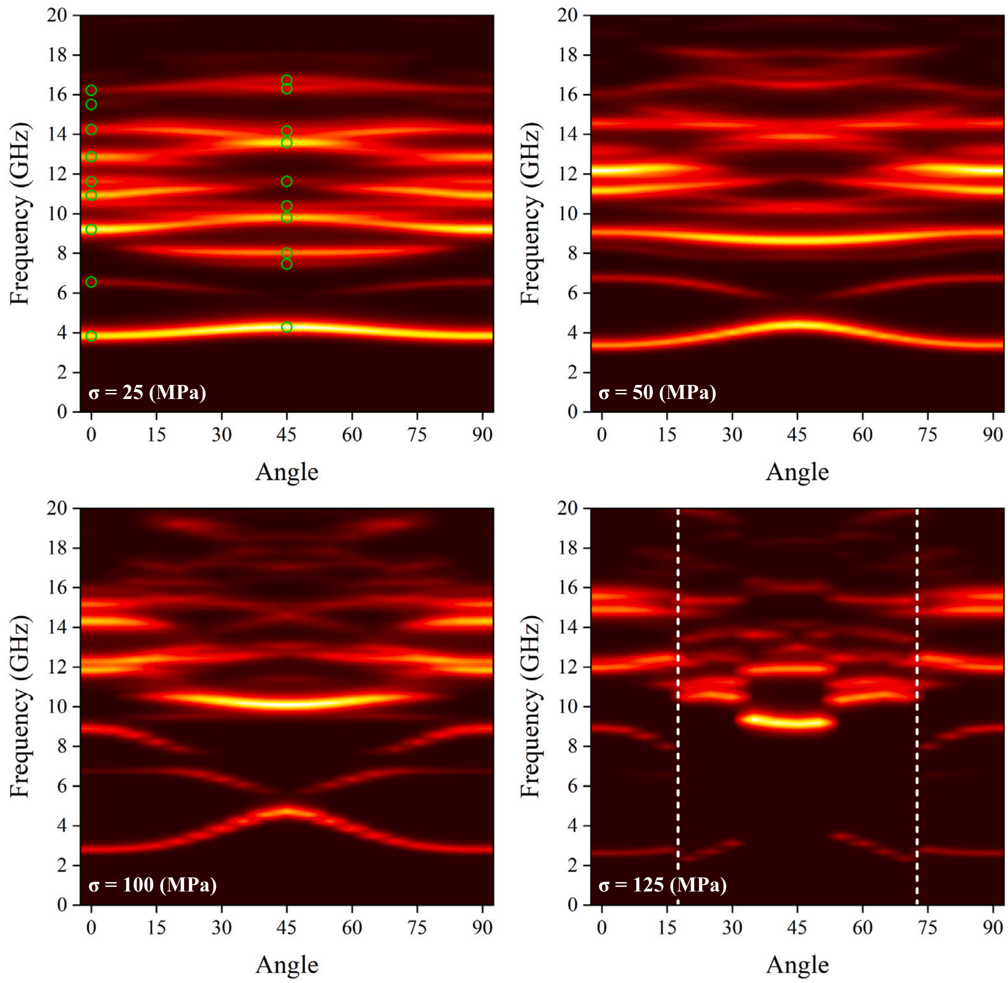

Fig. 4. Angular–frequency dispersion of the spin-wave modes of the antivortex state in a square FeGa nanodot under different stress magnitudes. The color maps represent the imaginary part of the dynamic susceptibility as a function of frequency and stress orientation angle θ for (a) σ = 25 MPa, (b) σ = 50 MPa, (c) σ = 100 MPa, and (d) σ = 125 MPa. Bright regions indicate resonance modes. At σ = 125 MPa, the white dashed vertical lines delimit the angular region where the antivortex becomes unstable.

of applied stress, the square geometry imposes an approximate fourfold symmetry, leading to standing spin-wave modes with diagonal nodal structures. The antivortex topology further modifies this symmetry by introducing a nonuniform magnetization distribution with converging and diverging in-plane components, which reshapes the internal effective field and results in mode profiles that differ from those of vortex states. As a consequence, the observed modes can be interpreted as diagonal standing-wave excitations with mixed symmetry character determined by the interplay between geometric confinement and antivortex topology.

Now we analyze the role of the stress orientation angle θ on the spin-wave dynamics for different stress magnitudes. Fig. 4 summarizes the resulting angular–frequency dispersion of the resonant modes, providing a comprehensive overview of the spin-wave response of the antivortex state. Figs. 4(a)–4(d) display the frequency spectra as a function of θ for σ = 25, 50, 100, and 125 MPa, respectively.

For the low-stress case σ = 25 MPa, the spin-wave spectrum exhibits a rich set of well-defined resonance branches spanning the entire angular range from $\theta = 0°$ to 90°, as shown in Fig. 4(a). A low-frequency resonance appears at approximately 4 GHz and shows a weak angular dispersion, characterized by a shallow maximum around $\theta \approx 45°$. At higher frequencies, several nearly parallel branches are observed in the range between 8 and 14 GHz, indicating the presence of multiple standing spin-wave modes with comparable spatial extent but different mode orders. Within this frequency window, the resonant branches display smooth and nearly symmetric angular dependence with respect to $\theta = 45°$, reflecting the relatively weak distortion of the antivortex configuration at low stress amplitude. Additional higher-frequency modes appear above 14 GHz, exhibiting reduced intensity and slightly enhanced angular curvature.

For the intermediate stress amplitude $\sigma = 50$ MPa, the spin-wave spectrum retains the multibranch character observed at lower stress, while exhibiting a noticeably enhanced angular modulation, as shown in Fig. 4(b). A low-frequency resonance remains in the vicinity of 4 GHz and shows a more pronounced angular dependence compared to the $\sigma = 25$ MPa case, with a broader curvature centered around $\theta \approx 45°$. In the intermediate frequency range, approximately between 8 and 14 GHz, the resonance branches display increased bending and reduced parallelism, indicating a stronger sensitivity of the spin-wave frequencies to the stress orientation. At higher frequencies, additional distortions of the resonance branches become evident, including the onset of mode bending and partial hybridization between neighboring modes. These features reflect the increased asymmetry of the antivortex configuration induced by the larger stress amplitude, as evidenced by the core displacement shown in Fig. 2(b).

For a higher stress amplitude of σ = 100 MPa, the spin-wave spectrum undergoes a pronounced reorganization, as illustrated in Fig. 4(c). Compared to the lower-stress cases, the resonance branches exhibit

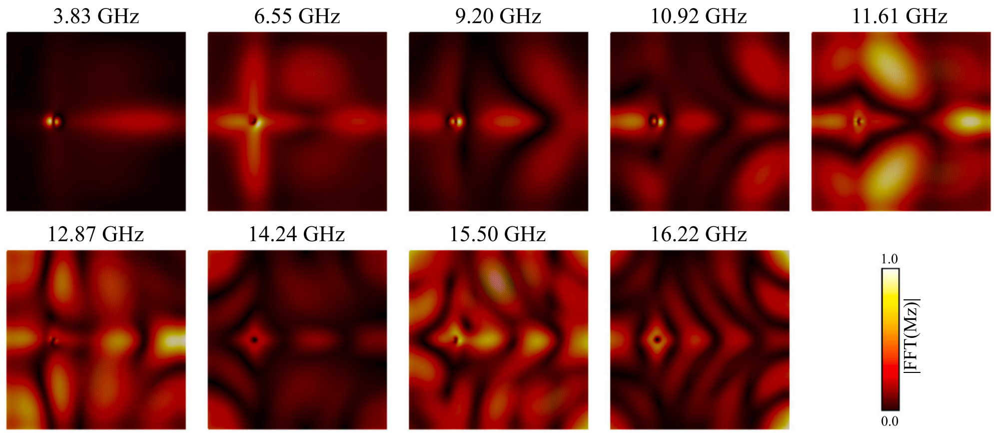

Fig. 5. Spatial profiles of the spin-wave modes for $\sigma = 25$ MPa and $\theta = 0°$.

strong angular modulation, with enhanced curvature and the appearance of clear anticrossing-like features in the intermediate frequency range.

This behavior reflects the progressive breaking of the fourfold symmetry imposed by the square geometry due to the stress-induced uniaxial anisotropy. The resulting symmetry reduction modifies the equilibrium magnetization configuration and allows coupling between spin-wave modes with different spatial symmetries, leading to the hybridization features observed in the spectra.

Several modes concentrate around the angular region $\theta \approx 45°$, where the stress-induced displacement of the antivortex core is maximal, leading to a significant redistribution of spectral intensity. In addition, the number of well-resolved resonance branches is reduced, particularly at higher frequencies, where mode merging and hybridization become evident. The angular dispersion is highly nonmonotonic, reflecting a substantial breaking of the fourfold symmetry of the nanodot.

For the highest stress amplitude, $\sigma = 125$ MPa, the spin-wave spectrum exhibits a qualitatively different behavior, as shown in Fig. 4(d). In contrast to the lower-stress regimes, a broad angular interval emerges in which the antivortex configuration becomes unstable. This region, delimited by the white dashed vertical lines, corresponds to the parameter range where the system relaxes into a non-antivortex magnetic state, in agreement with the phase diagram presented in Fig. 2(a). Within this angular interval, the spin-wave response is strongly modified, with the disappearance of well-defined resonance branches and the emergence of fragmented spectral features with reduced intensity. Outside this unstable region, where the antivortex state remains stable, the spectra recover a multibranch structure similar to that observed at lower stress amplitudes, albeit with enhanced angular distortion. These results demonstrate that, at sufficiently large stress, angular tuning not only reshapes the spin-wave spectrum but also drives a transition in the underlying magnetic configuration, leading to a qualitatively different dynamical response.

To gain deeper insight into the nature of the spin-wave modes, their spatial profiles were analyzed. Fig. 5 presents the spatial distributions of the resonant modes for $\sigma = 25$ MPa and $\theta = 0°$, obtained from the normalized FFT amplitude of the out-of-plane magnetization component.

The lowest-frequency mode at 3.83 GHz is strongly localized around the antivortex core, exhibiting an asymmetric intensity distribution elongated along a preferred in-plane direction. This mode corresponds to a core-dominated excitation with weak spatial extension across the nanodot. At 6.55 GHz, the spatial profile evolves into a more extended pattern, characterized by a cross-like asymmetry with pronounced intensity along the principal axes, indicating the onset of a collective excitation involving both the core region and the surrounding magnetization.

As the frequency increases to 9.20 and 10.92 GHz, the modes exhibit progressively more complex spatial structures, characterized by the appearance of regions with reduced oscillation amplitude and a redistribution of intensity away from the antivortex core toward the interior of the nanodot. In these modes, the oscillation pattern extends across the nanodot and develops preferred directions aligned with the square geometry, leading to curved boundaries separating regions of high and low intensity. This behavior reflects the combined effect of square confinement and symmetry breaking induced by the antivortex configuration. The mode at 11.61 GHz further enhances this complexity, showing several distinct regions of alternating intensity and a reduced degree of localization at the core.

For higher frequencies above 12 GHz, the modes become increasingly extended and spatially intricate. The profiles at 12.87 and 14.24 GHz show oscillations distributed over the entire nanodot, with multiple regions where the oscillation amplitude is strongly suppressed due to interference between counterpropagating spin waves. At even higher frequencies, such as 15.50 and 16.22 GHz, the spatial patterns display a larger number of such regions and pronounced interference effects, indicating highly excited standing spin-wave modes whose spatial structure is predominantly governed by geometric confinement.

Fig. 6 presents the spatial profiles of selected spin-wave modes for $\sigma = 25$ MPa at a stress orientation of $\theta = 45°$. In contrast to the $\theta = 0°$ case, the spatial patterns are significantly modified and exhibit a clear alignment along the diagonal direction of the nanodot, consistent with the imposed stress orientation. The lowest-frequency modes remain partially localized near the antivortex core; however, their spatial distribution becomes more asymmetric and elongated along the 45° direction.

At higher frequencies, the spin-wave modes develop increasingly extended and complex spatial structures, with intensity maxima and regions of suppressed oscillation predominantly arranged along the diagonal of the nanodot. This behavior indicates that a stress orientation of $\theta = 45°$ enhances the coupling between the antivortex configuration and the diagonal confinement imposed by the square geometry, leading to standing spin-wave modes whose spatial structure is governed by the combined effects of stress-induced anisotropy and geometric boundaries, as shown in Fig. 6.

Overall, Figs. 4–6 show that the stress angle provides a direct handle to reshape both the resonance spectrum and the spatial character of the antivortex spin-wave modes. Increasing σ enhances angular dispersion, promotes mode hybridization, and ultimately leads to spectral fragmentation near the instability region found in the state diagram. This close link between stability, core displacement, and mode structure motivates the conclusions presented next.

The proposed angular stress control can be experimentally implemented using piezoelectric substrates, where voltage-induced strain in

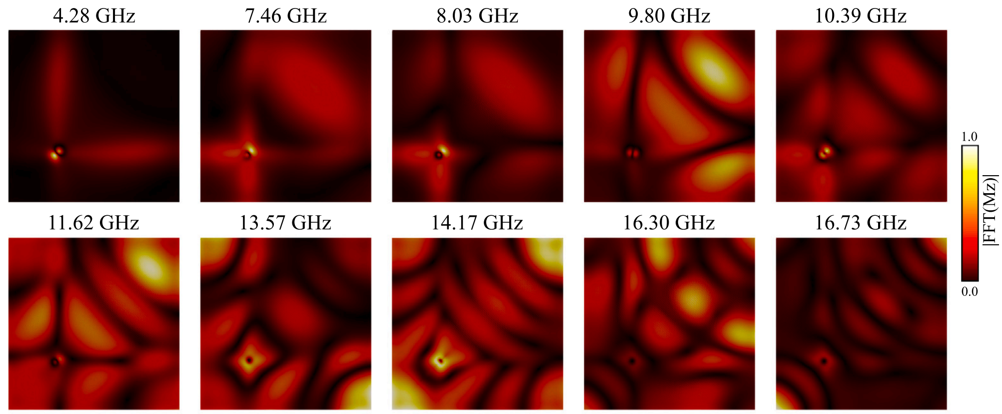

Fig. 6. Spatial profiles of the spin-wave modes for $\sigma = 25$ MPa and $\theta = 45°$.

the piezoelectric layer is transferred to the magnetic film. Patterned electrode arrays allow different electrode pairs to generate uniaxial strain along distinct in-plane directions, enabling directional control of the applied stress without mechanically rotating the sample [40]. In addition, experimental studies have shown that strain applied to the substrate can be efficiently transferred to FeGa films due to mechanical interlocking and chemical bonding at the interface [41]. For instance, in FeGa/PMN-PT heterostructures electric fields of about ± 4 kV/cm generate in-plane strains of approximately 0.19%, corresponding to stresses on the order of 100–150 MPa in the magnetic layer, which are comparable to the stress levels considered in this work [18,42].

Recent studies have further shown that electric-field-induced strain can be used to modulate the interfacial Dzyaloshinskii–Moriya interaction in multilayer systems such as Pt/Co/Pt, enabling voltage-controlled manipulation of chiral magnetic interactions and opening promising routes toward ultralow-power spintronic and magnonic devices [43]. These developments suggest that future hybrid multiferroic–magnonic platforms could exploit strain to simultaneously tune magnetoelastic anisotropy, chiral exchange interactions, and spin-wave propagation.

4. Conclusions

In conclusion, we have presented a comprehensive micromagnetic study of the angular dependence of stress-induced spin-wave dynamics in magnetic antivortices stabilized in square FeGa nanodots. By systematically varying both the magnitude and orientation of an in-plane uniaxial stress, we demonstrated that angular magnetoelastic anisotropy plays a crucial role in determining the stability, spatial position, and dynamic response of the antivortex configuration.

The magnetic state diagram reveals extended stability regions for the antivortex state, together with well-defined angular and stress thresholds beyond which the antivortex becomes unstable. Within the stable regime, the antivortex core exhibits pronounced angular-dependent displacements, indicating that stress orientation provides an efficient means to manipulate the internal structure of the antivortex without the application of external magnetic fields or electric currents.

The dynamic susceptibility analysis shows that the antivortex supports a discrete set of spin-wave modes whose frequencies and angular dispersion are strongly influenced by the stress orientation. At low and intermediate stress amplitudes, the spectra display multiple well-resolved resonance branches with smooth angular modulation, whereas at higher stress levels the spectra undergo a strong reorganization characterized by enhanced angular curvature, mode hybridization, and partial suppression of well-defined resonances in the vicinity of instability regions. Spatially resolved mode profiles reveal a transition from core-localized excitations at low frequencies to extended standing-wave modes governed by the interplay between square confinement and angular stress-induced anisotropy.

Overall, our results establish angular stress as a powerful and energy-efficient control parameter for tailoring both the stability and spin-wave dynamics of magnetic antivortices. This work provides fundamental insight into the magnetoelastic control of topological magnetic textures and highlights the potential of antivortex-based nanostructures as reconfigurable building blocks for future strain-controlled magnonic and spintronic devices.

CRediT authorship contribution statement

Eduardo Saavedra: Writing – review & editing, Writing – original draft, Visualization, Software, Resources, Methodology, Investigation, Formal analysis, Data curation, Conceptualization. **Helmunt Vigo-Cotrina:** Writing – review & editing, Writing – original draft, Software, Methodology, Investigation, Formal analysis, Conceptualization. **Mohammed Al Bahri:** Writing – review & editing, Methodology, Investigation, Formal analysis, Conceptualization. **Laura M. Pérez:** Writing – review & editing, Supervision, Resources, Methodology, Investigation, Formal analysis, Data curation. **Felipe Tejo:** Writing – review & editing, Validation, Supervision, Investigation, Conceptualization.

Declaration of competing interest

The authors declare the following financial interests/personal relationships which may be considered as potential competing interests: Felipe Tejo reports financial support was provided by Agencia Nacional de Investigación y Desarrollo (ANID). If there are other authors, they declare that they have no known competing financial interests or personal relationships that could have appeared to influence the work reported in this paper.

Acknowledgments

E.S. acknowledges partial financial support from FONDEF, Chile (Grant ID25I10641) and DICYT Regular 042631SD_REG.

L.M.P. acknowledges partial financial support from FONDECYT (Grant ID 1240985) and Centers of Excellence with BASAL/ANID (CIA250002, CEDENNA).

F.T. acknowledges financial support from ANID + Fondecyt de Iniciación en Investigación 2024 + 11241113.

M.A. acknowledges financial support from the Ministry of Higher Education, Research, and Innovation (MoHERI), Sultanate of Oman, under the Block Funding Program (Agreement No. BFP/RGP/ICT/23/032).

H. Vigo-Cotrina acknowledges financial support from Universidad Privada del Norte, Perú, under Project No 20241014.

Appendix A. Supplementary data

Supplementary material related to this article can be found online at https://doi.org/10.1016/j.jmmm.2026.174091.

Data availability

Data will be made available on request.

References

[1] D. Faurie, A.O. Adeyeye, F. Zighem, Prospects toward flexible magnonic systems, J. Appl. Phys. 130 (15) (2021).

[2] M Khelif, S Chiroli, N Challab, D Faurie, M Haboussi, F Zighem, Stress gradient effects on magnetic eigenmodes in ferromagnetic nanobars: a micromagnetic approach to magnetoelastic coupling, J. Phys. D: Appl. Phys. 58 (47) (2025) 475001.

[3] F. Tejo, E. Saavedra, J.C. Denardin, J. Escrig, Dynamic susceptibility of skyrmion clusters in Co/Pt nanodots, Appl. Phys. Lett. 117 (15) (2020).

[4] E. Saavedra, F. Tejo, N. Vidal-Silva, J. Escrig, Magnonic key based on skyrmion clusters, Sci. Rep. 11 (1) (2021) 23010.

[5] Felipe Tejo, Felipe Velozo, Ricardo Gabriel Elías, Juan Escrig, Oscillations of skyrmion clusters in Co/Pt multilayer nanodots, Sci. Rep. 10 (1) (2020) 16517.

[6] Junxiang Yao, Xiao Song, Xingsen Gao, Guo Tian, Peilian Li, Hua Fan, Zhifeng Huang, Wenda Yang, Deyang Chen, Zhen Fan, Min Zeng, Jun-Ming Liu, Electrically driven reversible magnetic rotation in nanoscale multiferroic heterostructures, ACS Nano 12 (7) (2018) 6767–6776.

[7] Jia-Mian Hu, Tiannan Yang, Long-Qing Chen, Strain-mediated voltage-controlled switching of magnetic skyrmions in nanostructures, Npj Comput. Mater. 4 (1) (2018).

[8] Supriyo Bandyopadhyay, Jayasimha Atulasimha, Anjan Barman, Magnetic straintronics: Manipulating the magnetization of magnetostrictive nanomagnets with strain for energy-efficient applications, Appl. Phys. Rev. 8 (4) (2021).

[9] Supriyo Bandyopadhyay, Perspective: There is plenty of room for magnetic straintronics in the analog domain, Npj Spintron. 2 (1) (2024).

[10] F. Zighem, D. Faurie, A review on nanostructured thin films on flexible substrates: links between strains and magnetic properties, J. Phys.: Condens. Matter. 33 (23) (2021) 233002.

[11] M.V. Sapozhnikov, R.V. Gorev, E.V. Skorokhodov, N.S. Gusev, A.V. Sadovnikov, O.G. Udalov, Zigzag domains caused by strain-induced anisotropy of the Dzyaloshinskii-Moriya interaction, Phys. Rev. B 105 (2) (2022).

[12] O.G. Udalov, R.V. Gorev, N.S. Gusev, A.V. Sadovnikov, M.V. Sapozhnikov, Electric field manipulation of the dzyaloshinskii–moriya interaction in hybrid multiferroic structures, IEEE Trans. Magn. 60 (11) (2024) 1–8.

[13] N.S. Gusev, A.V. Sadovnikov, S.A. Nikitov, M.V. Sapozhnikov, O.G. Udalov, Manipulation of the dzyaloshinskii–moriya interaction in Co/Pt multilayers with strain, Phys. Rev. Lett. 124 (15) (2020).

[14] Guohong Dai, Xiangjun Xing, Weichao Yan, Yun Shen, Xiaohua Deng, Stress tunable dynamic susceptibility of a magnetic vortex in a flexible Fe81Ga19 nanoring, J. Appl. Phys. 132 (4) (2022).

[15] Lele Peng, Shuhan Wan, Weichao Yan, Yun Shen, Xiaohua Deng, Guohong Dai, Stress tunable dynamic susceptibility of stripe domains in flexible FeGa films, AIP Adv. 15 (4) (2025).

[16] Xun Rao, Lele Peng, Weichao Yan, Yun Shen, Xiaohua Deng, Guohong Dai, Stress tunable spin dynamics of a magnetic vortex under resonant magnetic fields, AIP Adv. 15 (1) (2025).

[17] Guohong Dai, Xiangjun Xing, Yun Shen, Xiaohua Deng, Stress-controlled dynamic susceptibility in FeGa stripes, J. Appl. Phys. 123 (24) (2018).

[18] Eduardo Saavedra, Helmunt Vigo-Cotrina, Carlos Saji, David Laroze, Juan Escrig, Stress-tunable spin-wave dynamics in superellipse-shaped fega nanostructures, Appl. Phys. Lett. 127 (3) (2025).

[19] H. Vigo-Cotrina, Eduardo Saavedra, S. Urcia-Romero, S. Navarro-Vilca, A. P. Guimarães, Stress-tuned spin wave modes in magnetic vortex nanoellipses for flexible magnonic systems, Phys. B 723 (2026) 418113.

[20] K. Bublikov, J. Tóbik, A.V. Sadovnikov, M. Mruczkiewicz, Vortex gyrotropic mode in curved nanodots, J. Magn. Magn. Mater. 537 (2021) 168105.

[21] Iu.V. Vetrova, M. Zelent, J. Šoltýs, V.A. Gubanov, A.V. Sadovnikov, T. Šcepka, J. Dérer, R. Stoklas, V. Cambel, M. Mruczkiewicz, Investigation of self-nucleated skyrmion states in the ferromagnetic/nonmagnetic multilayer dot, Appl. Phys. Lett. 118 (21) (2021).

[22] Mateusz Zelent, Iuliia V. Vetrova, Jan Šoltýs, Xiaoguang Li, Yan Zhou, Vladislav A. Gubanov, Alexandr V. Sadovnikov, Tomas Šcepka, Jan Dérer, Roman Stoklas, Vladimír Cambel, Michal Mruczkiewicz, Skyrmion formation in nanodisks using magnetic force microscopy tip, Nanomaterials 11 (10) (2021) 2627.

[23] Felipe Tejo, Nicolas Vidal-Silva, Spin wave modes of antivortices hosted in square ultrathin nanodots, Chinese J. Phys. 98 (2025) 953–963.

[24] Felipe Tejo, Nicolas Vidal-Silva, Angular-selective spin wave modes of magnetic antivortices stabilized by anisotropic Dzyaloshinskii–Moriya interactions, J. Magn. Magn. Mater. 630 (2025) 173448.

[25] Xin Hu, X.S. Wang, Zhenyu Wang, Stabilization and dynamics of magnetic antivortices in a nanodisk with anisotropic Dzyaloshinskii-Moriya interaction, Phys. Rev. B 110 (1) (2024).

[26] A.A. Martyshkin, C.S. Davies, A.V. Sadovnikov, Magnonic interconnections: Spin-wave propagation across two-dimensional and three-dimensional junctions between yttrium iron garnet magnonic stripes, Phys. Rev. Appl. 18 (2022) 064093.

[27] Arne Vansteenkiste, Jonathan Leliaert, Mykola Dvornik, Mathias Helsen, Felipe Garcia-Sanchez, Bartel Van Waeyenberge, The design and verification of MuMax3, AIP Adv. 4 (10) (2014).

[28] Jonas J. Joos, Pedram Bassirian, Pieter Gypens, Jeroen Mulkers, Kai Litzius, Bartel Van Waeyenberge, Jonathan Leliaert, Tutorial: Simulating modern magnetic material systems in mumax3, J. Appl. Phys. 134 (17) (2023).

[29] P.E. Roy, In-plane anisotropy control of the magnetic vortex gyrotropic mode, Appl. Phys. Lett. 102 (16) (2013).

[30] Simone Finizio, Sebastian Wintz, Sebastian Gliga, Eugenie Kirk, Anna Kinga Suszka, Phillip Wohlhüter, Katharina Zeissler, Jörg Raabe, Unexpected field-induced dynamics in magnetostrictive microstructured elements under isotropic strain, J. Phys.: Condens. Matter. 30 (31) (2018) 314001.

[31] Guoliang Yu, Xiaofei Xu, Yang Qiu, Han Yang, Mingmin Zhu, Haomiao Zhou, Strain-modulated magnetization precession in skyrmion-based spin transfer nano-oscillator, Appl. Phys. Lett. 118 (14) (2021).

[32] Guohong Dai, Qingfeng Zhan, Yiwei Liu, Huali Yang, Xiaoshan Zhang, Bin Chen, Run-Wei Li, Mechanically tunable magnetic properties of Fe81Ga19 films grown on flexible substrates, Appl. Phys. Lett. 100 (12) (2012) 122407.

[33] Xiaoshan Zhang, Qingfeng Zhan, Guohong Dai, Yiwei Liu, Zhenghu Zuo, Huali Yang, Bin Chen, Run-Wei Li, Effect of buffer layer and external stress on magnetic properties of flexible FeGa films, J. Appl. Phys. 113 (17) (2013).

[34] Eduardo Saavedra, Felipe Tejo, Nicolas Vidal-Silva, Juan Escrig, Symmetry breaking-induced resonance dynamics in Bloch point nanospheres: Unveiling magnetic volume effects and geometric parameters for advanced applications in magnetic sensing and spintronics, ACS Appl. Mater. & Interfaces 16 (21) (2024) 27605–27613.

[35] J Fullerton, A Hierro-Rodriguez, C Donnelly, D Sanz-Hernández, L Skoric, D.A. MacLaren, A Fernández-Pacheco, Controlled evolution of three-dimensional magnetic states in strongly coupled cylindrical nanowire pairs, Nanotechnology 34 (12) (2023) 125301.

[36] Sergi Lendinez, Mojtaba T. Kaffash, Olle G. Heinonen, Sebastian Gliga, Ezio Iacocca, M. Benjamin Jungfleisch, Nonlinear multi-magnon scattering in artificial spin ice, Nat. Commun. 14 (1) (2023).

[37] N. Noginova, V. Gubanov, M. Shahabuddin, Yu. Gubanova, S. Nesbit, V.V. Demidov, V.A. Atsarkin, E.N. Beginin, A.V. Sadovnikov, Ferromagnetic resonance in permalloy metasurfaces, Appl. Magn. Reson. 52 (7) (2021) 749–758.

[38] Changting Dai, Kaile Xie, Zizhao Pan, Fusheng Ma, Strong coupling between magnons confined in a single magnonic cavity, J. Appl. Phys. 127 (20) (2020).

[39] Oleksandr V. Dobrovolskiy, Sergey A. Bunyaev, Nikolay R. Vovk, David Navas, Pawel Gruszecki, Maciej Krawczyk, Roland Sachser, Michael Huth, Andrii V. Chumak, Konstantin Y. Guslienko, Gleb N. Kakazei, Spin-wave spectroscopy of individual ferromagnetic nanodisks, Nanoscale 12 (41) (2020) 21207–21217.

[40] Ayan Kumar Biswas, Hasnain Ahmad, Jayasimha Atulasimha, Supriyo Bandyopadhyay, Experimental demonstration of complete 180° reversal of magnetization in isolated co nanomagnets on a PMN–PT substrate with voltage generated strain, Nano Lett. 17 (6) (2017) 3478–3484.

[41] Guohong Dai, Qingfeng Zhan, Huali Yang, Yiwei Liu, Xiaoshan Zhang, Zhenghu Zuo, Bin Chen, Run-Wei Li, Controllable strain-induced uniaxial anisotropy of Fe81Ga19 films deposited on flexible bowed-substrates, J. Appl. Phys. 114 (17) (2013).

[42] P.B. Meisenheimer, R.A. Steinhardt, S.H. Sung, L.D. Williams, S. Zhuang, M.E. Nowakowski, S. Novakov, M.M. Torunbalci, B. Prasad, C.J. Zollner, Z. Wang, N.M. Dawley, J. Schubert, A.H. Hunter, S. Manipatruni, D.E. Nikonov, I.A. Young, L.Q. Chen, J. Bokor, S.A. Bhave, R. Ramesh, J.-M. Hu, E. Kioupakis, R. Hovden, D.G. Schlom, J.T. Heron, Engineering new limits to magnetostriction through metastability in iron-gallium alloys, Nat. Commun. 12 (1) (2021).

[43] Shen Li, Suteng Zhao, Dion M.F. Hartmann, Wei Yang, Xiaoyang Lin, Weisheng Zhao, Reinoud Lavrijsen, Modulation of the dzyaloshinskii–moriya interaction in Pt/Co/pt with electric field induced strain, Appl. Phys. Lett. 126 (16) (2025).